Title

Increase of the Catalytic Activity of Molten Salts by Doping: Methane Activation

Journal

The Journal of Physical Chemistry C, 128(1)

ISSN

1932-7447

Authors

Dutta, Sajal Kanti

Singh, Baljit

Metiu, Horia

et al.

Publication Date

2024-01-11

DOI

10.1021/acs.jpcc.3c07024

The Increase of the Catalytic Activity of Molten Salts By Doping: Methane Activation

Sajal Kanti Dutta[†], Baljit Singh[†], Horia Metiu[¶,*], Vishal Agarwal[†,‡,*]

[†]Department of Chemical Engineering, Indian Institute of Technology Kanpur; Kanpur 208016, India

[‡]Department of Sustainable Energy Engineering, Indian Institute of Technology Kanpur; Kanpur 208016, India

[¶]Department of Chemistry and Biochemistry, University of California Santa Barbara; Santa Barbara, California 93106-9510, United States

*Corresponding author. Email: metiu@chem.ucsb.edu; vagarwal@iitk.ac.in

ABSTRACT: A melt containing 1% $FeCl_3$ and 99% KCl is a good catalyst for methane pyrolysis, while molten KCl has almost no catalytic activity. We use *ab initio* molecular dynamics, based on density functional theory, to examine why this surprising behavior takes place. We find that in this ionic salt, the charge on the iron fluctuates between Fe^{3+} and Fe^{2+} and the conversion to Fe^{2+} takes charge from several chlorine ions which become active for methane dissociation. We speculate that such activation is general and takes place for any dopant M^{n+} which has a state $M^{(n-1)+}$.

1. INTRODUCTION

Hydrogen is a commodity chemical used for producing ammonia, methanol, and petroleum products and for hydrogenating organic compounds. It is an environmentally friendly fuel, which might become an important factor in future "green economy". Currently, about 95% of hydrogen is manufactured by steam methane reforming (SMR),[1] a process that generates CO_2 as a side product; the production of 1 million standard cubic feet (SCF) of hydrogen generates 250,000 standard cubic feet of CO_2. In a green economy, the use of the hydrogen produced by this method would require CO_2 sequestration, a process that is expensive and problematic.

One possibility for "green" hydrogen production is the endothermic methane pyrolysis reaction

$$CH_4 \leftrightarrow C + 2H_2$$

If a fraction of the hydrogen produced is burned, to provide the heat of reaction, this process produces no CO_2. Approximate economic analysis suggests that the process will be economically competitive with SMR if future legislation imposes a penalty on CO_2 production or demands CO_2 sequestration.[2]

The gas-phase pyrolysis reaction is slow and requires high temperature, and the carbon produced by reaction clogs the equipment. The conventional heterogeneous catalysts (e.g. supported Ni) are deactivated by carbon deposition. One can burn off the carbon to regenerate the catalyst but this produces CO_2.

In order to avoid catalyst deactivation several groups have proposed performing methane pyrolysis by using a molten catalyst in a bubble column reactor. Methane is introduced, through a sparger, at the bottom of the column and the pyrolysis reaction takes place in the bubbles traveling upwards through the melt. The carbon product is trapped in the bubbles and is transported to the top of the molten catalyst where it floats and can be removed. The catalyst is not deactivated by coking because the bubbles entering the reactor encounter clean catalyst. Several recent articles[3-7] have reviewed this kind of work.

Recent experiments[8] on methane pyrolysis have reported two surprising findings. (1) The addition of 1wt% $FeCl_3$ to a molten KCl/NaCl eutectic lowers the apparent activation energy for pyrolysis from 301 kJ/mol for KCl/NaCl, to 178 kJ/mol for $FeCl_3$/NaKCl. (2) Increasing the concentration of $FeCl_3$ from 1 wt% to 7 wt% has almost no effect on the catalytic activity. It is not clear why the effectiveness of the catalyst does not increase with the concentration of the iron promoter.

This behavior of $FeCl_3$/KCl is unlike that of other halides. We have found, by DFT calculations, that dissolving a small amount of $AlCl_3$ in molten KCl has hardly any effect on the activation energy for pyrolysis. A study of the $MnCl_2$/KCl melt found[9] that the mixture is more active than either pure molten KCl or pure molten $MnCl_2$. However, unlike in the case of $FeCl_3$/KCl, a small amount of $MnCl_2$ has a very small effect on catalytic activity and the activity increases as the concentration of $MnCl_2$ is increased beyond 1%.

In this work we used *ab initio* molecular dynamics, with forces derived from density functional theory, to investigate the reasons for the peculiar catalytic activity of $FeCl_3$/KCl. We have found several properties that explain the remarkable behavior of this catalyst. (1) Fe^{3+} prefers to be in the bulk of the KCl melt, not on the surface; it is therefore intriguing that its addition to the KCl melt strongly affects the catalytic activity. (2) Even when we force Fe^{3+} to stay on the surface of the melt, it is not a catalytic site; CH_4 does not dissociate on it. (3) Methane dissociates with a low activation energy on the surface of $FeCl_3$/KCl, at many sites that are not adjacent to the iron ion. (4) As the time evolves during the simulation, the iron forms and unforms a variety of complex negative ions of the form $FeCl_n^{-m}$. In some of them, iron has a charge of 2+. (5) To form these complexes, iron takes electron charge from several Cl^-ions and activates them. (6) The dissociation of methane is catalyzed by these charge-deficient chlorine ions.

This scenario allows us to understand why adding a small amount of $AlCl_3$ or $MnCl_2$ to KCl causes only a minor improvement in catalytic activity of the melt. We found that, like in the case of $FeCl_3$, $AlCl_3$, and $MnCl_2$ form complex negative ions when dissolved in KCl. However, in all these complexes the aluminum charge is 3+ and the manganese charge is 2+; in these systems complex formation does not cause a change in the charge of the surrounding chlorine ions and these complexes do not activate the chlorine to promote CH_4 dissociation. Preliminary calculations examining a $MoCl_5$/KCl melt predict that $MoCl_5$ will behave like $FeCl_3$.

2. COMPUTATIONAL METHODS

We have performed *ab initio* constant-temperature molecular dynamics simulations (AIMD) to investigate the catalytic activity of a $FeCl_3$/KCl melt for methane pyrolysis. Simulations were also performed to illustrate that a melt of $AlCl_3$/KCl is inactive.

All simulations examined a liquid layer containing 50 K^+ ions, 50 Cl^- ions, and one $FeCl_3$ or $AlCl_3$ molecule in a simulation box of 15Å×15Å×40Å. The concentration of $FeCl_3$ corresponds to that used in experiments.[8] The same concentration was used for $AlCl_3$/KCl. The simulation cell was periodically repeated in all three directions. Because of the presence of a vacuum region above the liquid the model mimics a thin liquid film.

Spin-polarized density function theory (DFT) calculations and molecular dynamics (MD) simulations were performed using the CP2K (version 8.2) software package.[10] For several benchmarking calculations, we used Gaussian16.[11] DFT calculations were performed with the generalized gradient approximation (GGA) with Perdew, Burke and Ernzerhoff (PBE)[12] exchange correlation functional. A mixed Gaussian and plane-wave basis set[13] was used with an energy cutoff of 320 Ry. The cutoff was determined by benchmarking and the total energy was converged within 0.015 eV. The core electrons were represented by Goedecker-Teter-Hutter (GTH) pseudo-potential,[14] and a double-zeta basis-set with one set of polarization function (DZVP)[15] was used for the valence electrons. The self-consistent field iteration was terminated when the change in energy was less than 8×10^{-5} eV. A van der Waals correction was added by using the Grimme's D3 method.[16] We found that the dissociation energy of KCl calculated with PBE/DZVP is close to that obtained when using Becke 3-parameter exchange functional[17] and Lee-Yang-Parr correlation functional[18] as tabulated in Table S1 (Supplementary Information).

To determine the lowest energy spin state, we performed calculations with gas-phase $FeCl_3$ and $KFeCl_4$. We found that the spin multiplicity of the lowest energy state was six[19] (see Table S2, Supplementary Information); therefore, the liquid $FeCl_3$/KCl system was modeled as a sextet. Because there are no unpaired electrons in pure KCl and $AlCl_3$, $AlCl_3$/KCl was modeled as a singlet.

In order to diminish the self-interaction error of DFT, we used a hybrid functional or a DFT+U correction.[20] Because hybrid functionals require large computing power, we used them only for benchmarking small systems. For liquid films we used DFT+U with U = 2.5 eV for the d-orbitals of Fe atom. This value was chosen because it fits the magnetic moments on Fe in the gas-phase $KFeCl_4$ calculated with the B3LYP functional (see Figure S1, Supplementary Information). Nearly the same U value was obtained when fitting the magnetic moments of Fe in the gas-phase K_2FeCl_4 and $FeCl_3$.

The *ab initio* molecular dynamics (AIMD) simulations were performed in the NVT ensemble, and the equations were numerically integrated with a time step of 1 fs. We used the extended Lagrangian formulation of Nosé-Hoover chain thermostat[21] with a chain length of 3, to maintain the canonical distribution at 1000 °C. The initial state of the $FeCl_3$ (or $AlCl_3$) in bulk KCl melt was generated by creating a cavity in the middle of an equilibrated KCl molten film and inserting a molecule of $FeCl_3$ (or $AlCl_3$) in the center of the cavity. The system was then equilibrated in two steps. In the first step we performed, for 10 picoseconds, an AIMD simulation in which only the K^+ and Cl^- ions located at less than 6 Å from the Fe (or Al) ion were allowed to move. In the second step we performed, for 10 ps, an AIMD simulation in which all ions moved. The configuration

obtained after these two runs served as an initial state for further investigation. Similarly, in a simulation in which the $FeCl_3$ molecule was forced to remain at the surface of the film, we allowed the ions within the first two layers away from Fe to move until the system reached thermal equilibrium.

We calculated the mean total energy of the liquid by using

$$\langle E \rangle = \frac{1}{t - t_0} \int_{t_0}^{t} E(\tau) d\tau \quad (1)$$

where $E(\tau)$ is the total energy of the film at time τ. The equilibration time t was 20 ps for all runs. Data were taken for 15 ps after the equilibration.

We found that the average energy of the molten $FeCl_3$/KCl, when the Fe is in the bulk of the film, is lower by ~0.6 eV than the energy calculated with the Fe-complex on the surface of the KCl melt (see Figure S2, Supplementary Information).

The optimum ion positions were found by using the Broyden-Fletcher-Goldfarb-Shanno (BFGS) algorithm.[22] The ionic loop was terminated when the force on each ion was less than 0.02 eV/Å. The net charges on the ions were computed using the density-derived DDEC6 method,[23-25] which is based on partitioning the electronic probability density to approximately reproduce the electrostatic potential. The spin moment was computed by using Mulliken spin populations. Calculations on gas-phase $FeCl_3$, $KFeCl_4$, K_2FeCl_4, and metal halide clusters as tabulated in Tables S3, S4, and S5, (Supplementary Information) suggest that Mulliken spin moments slightly overestimate those obtained from DDEC6, but the qualitative trends are the same. For these calculations and for the transition-state calculations we used a plane wave cutoff of 350 Ry and terminated the self-consistent field (SCF) cycle when the energy change which was below 3×10^{-6}eV.

The barriers for CH_4 dissociation on the molten $FeCl_3$/KCl surface were computed using the nudged elastic band (NEB) method.[26] These calculations require one to specify an initial state and the final state after dissociation. Interesting complications are present when the surface is liquid because the ion positions and therefore the activation energy for dissociation are different at different surface sites. To calculate these activation energies, we proceeded as follows. We selected at random twelve ionic configurations (from a sample with Fe in +2 state) from molecular dynamics run of 40 ps. For each random configuration, the bottom 75% of the ions in the molten slab were frozen and the upper 25% were allowed to relax to minimize the energy. This creates a "glassy" surface structure mimicking that of a liquid slab. The nudged elastic band (NEB)[26] was used to calculate the activation energy for methane dissociation at various sites on these solid glassy surfaces. The initial guess of the images on the NEB path was generated via a linear interpolation between the reactant and the product configurations. Often, linear interpolation results in atoms that are too close to each other. This leads to high forces on the respective images and sometimes convergence failure of the NEB pathway. Therefore, the initial guess of images was manually refined to keep the C and H atoms apart by at least 0.9 Å. The minimum energy path was pre-optimized with the improved-tangent (IT) NEB method and the transition state was finally revised with the climbing-image NEB (CI-NEB).[27] The CI-NEB optimization was terminated when the maximum NEB force on each image was less than 0.02 eV/Å. In all cases, we required eight to ten images to map out the minimum energy path for dissociation.

The average structure of KCl melt, $FeCl_3$/KCl melt, and $AlCl_3$/KCl melt was characterized by radial pair-distribution functions g(r) was defined by

$$p_{ij}(r)\, dr = 4\, \pi\, r^2\, g_{ij}(r)\, \rho\, dr \qquad (2)$$

where $p_{ij}(r)dr$ is the probability of finding the ion j at a distance between r and r+dr from the ion i, and ρ is the density. We have calculated the pair-distribution function by dividing the liquid layer into bins of constant width (δr = 0.1 Å) and then generating a histogram of the distances between pairs of atoms. For pure KCl melt, the averages were computed for ions which remained near the center of film for the entire simulation time. The K-Cl pair distribution function shows a peak at a distance of 3.05 Å (Figure S3A, Supplementary Information). The integration of K-Cl pair distribution function (r < 5.0 Å) gave us an average of 6.2 Cl nearest-neighbors of K. Neutron diffraction studies on molten KCl at 800 °C have reported that Cl-K nearest neighbor peaks at 3.06 Å and Cl has 6.1 K ions as nearest-neighbors.[28] We are not aware of any experimental studies at 1000 °C.

The radial pair distribution function multiplied by the average number density is plotted in Figure S3B, Supplementary Information. In molten $FeCl_3$/KCl, we find Fe-Cl and Fe-K nearest-neighbor peaks at 2.3 Å and 4.3 Å, respectively. Integration of Fe-Cl pair distribution function yields an average of 4.04 Cl ions in the first coordination shell (r < 3.2 Å). In the inset of Figure S3B, we also plot Fe(II)-K and Fe(III)-K radial distribution function multiplied by the average number density. The nearest-neighbor peaks for these pairs are at distance 4.1 Å and 4.6 Å, respectively. The shifting of Fe-K nearest-neighbor peak for Fe(III) ion suggests that K atoms are more closely packed in the second coordination shell when the Fe ion is in +2 oxidation state, as one would expect.

The Al-Cl pair-distribution function times the average atomic density in the $AlCl_3$/KCl melt shows a sharp peak at 2.2 Å (Figure S3C, Supplementary Information), and integration of Al-Cl pair-distribution function, within a cutoff distance of 3 Å, yields an average of 4 Cl ions surrounding an Al ion. The peak distance matches closely that reported experimentally for $AlCl_3$ in alkali halide melts.[29]

An interesting feature in Figure S3 B and C (Supplementary Information) is that the radial pair-distribution function goes to zero after attaining a first maximum, suggesting the presence of a stable complex. Since radial pair-distribution function is an average quantity, it does not reflect the dynamic changes in the Fe-Cl (Al-Cl) complex in the KCl melt. We investigate the nature of this complex by plotting coordination number of Fe ion with Cl ions, the charge on the complex and the spin moment on the complex as functions of time. We compute the coordination number (CN) of ion A with ion B in the molten salt using

$$CN = \frac{1-\left(\frac{R_{AB}-D_0}{R_0}\right)^6}{1-\left(\frac{R_{AB}-D_0}{R_0}\right)^{12}} \qquad (3)$$

R_0 and D_0 are empirical parameters having units of length. R_{AB} is the distance between ion A and ion B. With the above functional form, the value of CN is 0.5 at $R0+D_0$. For $FeCl_3$/KCl system, we used R_0 = 1.7 Å and D_0 = 1.5 Å; for $AlCl_3$/ KCl system we used R_0=1.7 Å and D_0 = 1.4 Å.

3. RESULTS AND DISCUSSION

We have used *ab initio* molecular dynamics with forces derived from density functional theory to calculate the positions of the ions and the energy of a slab containing 50 K^+ ions, 50 Cl^- ions, and one $FeCl_3$ molecule. The concentration of $FeCl_3$ in this system is close to that used in the experiments.[8] Periodic boundary conditions have been used in all three directions. Details regarding the choice of functional and of the basis set used in these calculations are given in the Computational Methods section.

The simulations show that a $FeCl_3$ molecule added to the KCl slab dissociates and the Fe ion produced by dissociation moves into the bulk of the slab. Fe^{3+} prefers to be away from the surface and therefore it is not in contact with methane. As explained earlier, the iron ion forms transient negative ions of the form $FeCl_n^{-m}$. To detect these complexes in the simulation we have monitored the number of chlorine ions near the Fe ion (the coordination number), the magnetic moment, and the charge on the Fe ion. The results are shown in Figure 1.

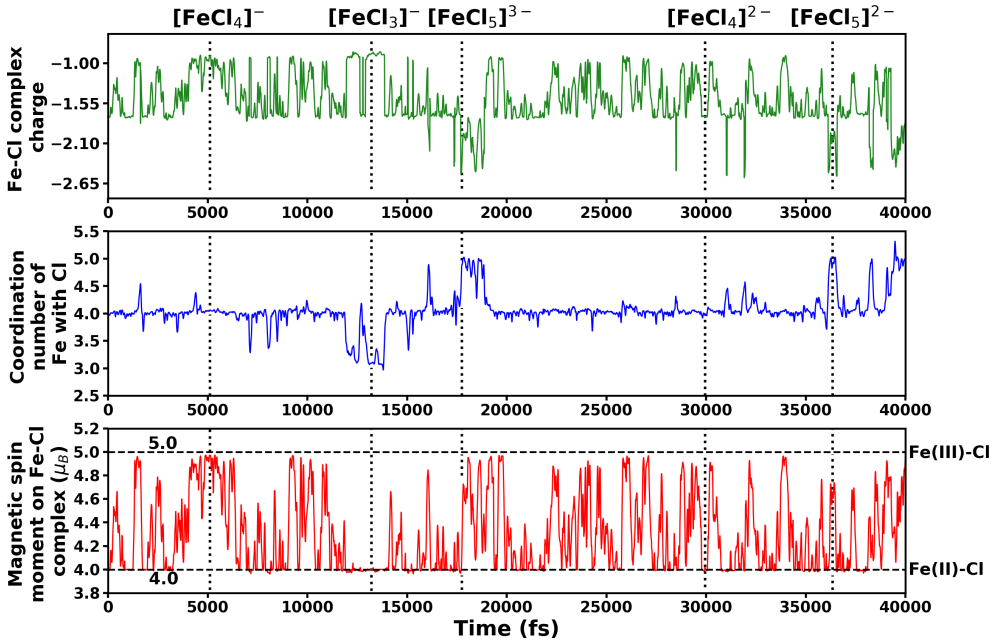

Figure 1. The charge on the iron, the number of halogens around iron (the coordination number), and the magnetic spin moment on the iron. At the top of the graph we indicate the complexes formed at different times.

The evolution of the coordination number tells us that iron forms and unforms the complex ions $FeCl_4^-$ and $FeCl_5^{2-}$, in which the charge of the iron is 3+, and the ions $FeCl_3^-$, $FeCl_5^{3-}$, and $FeCl_4^{2-}$ in which the charge of the iron is 2+. To change its charge from 3+ to 2+, iron extracts electronic charge from *several* chlorine ions. The dissociation of CH_4 takes place on those chlorine ions having a diminished charge. We note that this mechanism is different from Shilov's reaction,[30] wherein a platinum complex dissolved in water activates methane. In Shilov's reaction oxygen is involved, which is not the case with our pyrolysis reaction. Our reaction takes place at temperatures above 800 ºC, whereas Shilov is a low-temperature reaction. The Pt catalyst in Shilov's reaction directly participates in the reaction, which is not the case here.

The activation energy E_a for the dissociation of methane and the dissociation energy ΔE are difficult to calculate when the surface of the catalyst is liquid. The ions have different configurations at different surface sites and the configuration at any given place on the surface changes in time. To deal with this situation we performed *ab initio* molecular dynamics simulations with the $FeCl_3$/KCl slab and selected at random 12 configurations in which the charge of iron was Fe^{2+}. Then we froze the bottom 75% of the ions and relaxed the top 25% to minimize the energy. The resulting solid has the "glassy" structure of the liquid. We then used the nudged elastic band method (see Computational Methods for details) to calculate the activation energy. When calculating the activation energy by the nudged elastic band method, 25% of the atoms are allowed to adjust as the reaction coordinate changes. Figure 2 shows an energy level diagram with the activation energy for methane dissociation and the binding energy of the dissociation fragments. The dispersion of these two quantities is large: the smallest activation energy is 128 kJ/mol and the highest is 194 kJ/mol. The measured effective activation energy is ~170 kJ/mol.[8] Similar dispersion is obtained for the binding energy of the dissociation fragments. We note that E_a and ΔE in this system do not obey the Brønsted-Evans-Polanyi rule, which states that the larger the binding energy of the fragments the smaller the activation energy. We provide a movie of CH_4 dissociation on $FeCl_3$/KCl surface, with a barrier of 133 kJ/mol, in the Supporting Information. We provide C-Cl distances and C-Fe distances for the reaction in Figure S4 (Supporting Information). Fe in the melt remains more than 12 Å away from the carbon atom during the reaction. We also computed reaction energies by forcing Fe to be on the surface of the melt (see Figure S5, Supporting Information), which comes out to be more than 200 kJ/mol, suggesting that Fe does not directly participate in the reaction.

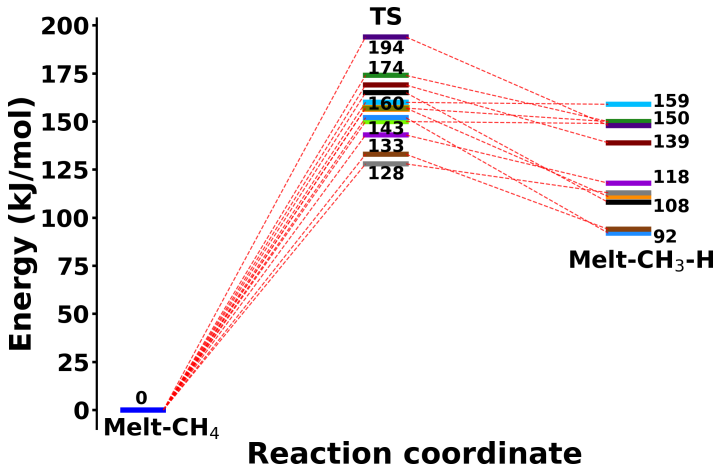

Figure 2. The activation energy for methane dissociation and the binding energy of the H and CH_3 fragments in $FeCl_3$/KCl melt.

We have also studied, by a similar procedure, the behavior of a slab of KCl in which we have introduced $AlCl_3$. We found that $AlCl_3$ makes various complex ions but in all of them Al is 3+ (see Figure S6, Supplementary Information). This is consistent with the fact that, unlike Fe, Al does not make salts in which Al is 2+. Therefore, according to the qualitative picture proposed here the addition of $AlCl_3$ to KCl should not activate the salt for methane dissociation. Our calculations found that the dissociation energy to form H and CH_3 bound to the surface is in the range of 308–339 kJ/mol (see Figure S7, Supplementary Information). The activation energy for

dissociation must be larger than this value; therefore, adding $AlCl_3$ does not activate KCl. Simulations of $MnCl_2$/KCl found the same thing: Mn makes several complexes but in all of them Mn has the charge 2+ (see Figure S8, Supplementary Information). According to our model this means that a very small amount of $MnCl_2$ will not substantially change the activity of the $MnCl_2$/KCl catalyst. This is what the experiments have found.[9]

4. CONCLUSIONS

We *speculate* that the pattern described here may be general. One can activate a chemically inert (e.g. KCl, NaCl) molten salt by doping it with a small amount of another salt. The cation of the dopant must be in a high charge state (e.g. Fe^{3+}, Mo^{5+}) and be reducible to a lower charge state (e.g. $Fe^{3+}$to Fe^{2+}, Mo^{5+} to Mo^{4+}). The presence of such redox couples will activate the anion of the inert salt solvent. It is conceivable that this procedure will activate other anions besides Cl^-. The ability of iron to fluctuate between Fe^{3+} and Fe^{2+}, when dissolved in molten KCl, may correlate with the free energy given by the Nernst equation for the Fe^{2+}-Fe^{3+} couple and should form an appropriate descriptor for identifying dopants. This is an apt subject for future exploration. Most of the available literature is on standard electrode potential in water solution, which may not be an appropriate descriptor because the solvation energies in molten salts are not the same as in water.

Acknowledgments. S.K.D. thanks IIT Kanpur for financial support under the Institute Post-doctoral Fellowship. V.A. acknowledges financial support from the Science and Engineering Board (SERB), Ramanujan Fellowship and grant no. IPA/2021/000031. The authors also acknowledge the support of DST, Govt. of India, for the High-Performance Computing (HPC2013 and ParamSanganak) facility at IIT Kanpur.

Supporting Information Available. Gas-phase benchmarking calculations; determination of U value; comparison of average energy of $FeCl_3$/KCl melt when iron is in bulk vs that on the surface; pair-distribution functions, C-Cl and C-Fe distances, reaction energies of CH_4 dissociation when Fe is on the surface of KCl melt (PDF). Movie of the minimum energy pathway for methane dissociation (AVI).

Notes

The authors declare no competing financial interest.

References

(1) Bartolomew, C. H.; Farrauto, R. J. *Fundamentals of Industrial Catalytic Processes.* Wiley & Sons, New York, 2011.

(2) Parkinson, B.; Matthews, J. W.; McConnaughy, T. B.; Upham, C. D.; McFarland, E. W. Techno-economic analysis of methane pyrolysis in molten metals: decarbonizing the natural gas. *Chem. Eng. Technol.***2017**, *40*, 1022-1030.

(3) Msheik, M.; Rodat, S.; Abanades, S. Methane cracking for hydrogen production: A review of catalytic and molten media pyrolysis. *Energies* **2021**, *14*, 3107.

(4) Fan, Z.; Weng, W.; Zhou, J.; Gu, D.; Xiao, W. Catalytic decomposition of methane to produce hydrogen: A review. *J. Energy Chem.***2021**, *58*, 415-430.

(5) Chen, L.; Qi, Z.; Zhang, S.; Su, J.; Somorjai, G. A. Catalytic hydrogen production from methane: A review on recent progress and prospect.*Catalysts* **2020**, *10*, 858.

(6) Sánchez-Bastardo, N.; Schlögl, R.; Ruland, H. Methane pyrolysis for zero-emission hydrogen production: A potential bridge technology from fossil fuels to a renewable and sustainable hydrogen economy. *Ind.Eng.Chem.Res.* **2021**, *60*, 11855-11881.

(7) Zuraiqi, K.; Zavabeti, A.; Allioux, F.-M.; Tang, J.; Nguyen, C. K.; Tafazolymotie, P.; Mayyas, M.; Ramarao, A. V.; Spencer, M.; Shah, K.; et al. Liquid metals in catalysis for energy applications. *Joule* **2020**, *4*, 2290-2321.

(8) Kang, D.; Palmer, C.; Mannini, D.; Rahimi, N.; Gordon, M. J.; Metiu, H.; McFarland, E. W. Catalytic methane pyrolysis in molten alkali chloride salts containing iron. *ACS Catal.* **2020**, *10*, 7032-7042.

(9) Kang, D.; Rahimi, N.; Gordon, M. J.; Metiu, H.; McFarland, E. W. Catalytic methane pyrolysis in molten $MnCl_2$-KCl. *Appl. Catal. B: Environ.* **2019**, *254*, 659-666.

(10) Hutter, J.; Iannuzzi, M.; Schiffmann, F.; Vandevondele, J. Cp2k: Atomistic simulations of condensed matter systems. *Wiley Interdiscip. Rev.: Comput. Mol. Sci.* **2014**, *4*, 15-25.

(11) Frisch, M. J.; Trucks, G. W.; Schlegel, H. B.; Scuseria, G. E.; Robb, M. A.; Cheeseman, J. R.; Scalmani, G.; Barone, V.; Petersson, G. A.; Nakatsuji, H.; et al. Gaussian 16 Rev. C.01, Wallingford, CT, 2016.

(12) Perdew, J. P.; Burke, K.; Ernzerhof, M. Generalized gradient approximation made simple. *Phys. Rev. Lett.* **1996**, *77*, 3865-3868.

(13) Vandevondele, J.; Krack, M.; Mohamed, F.; Parrinello, M.; Chassaing, T.; Hutter, J. Quickstep: Fast and accurate density functional calculations using a mixed Gaussian and plane waves approach. *Comput. Phys. Commun.* **2005**, *167*, 103-128.

(14) Hartwigsen, C.; Gøedecker, S.; Hutter, J. Relativistic separable dual-space Gaussian pseudopotentials from H to Rn. *Phys. Rev. B* **1998**, *58*, 3641.

(15) VandeVondele, J.; Hutter, J. Gaussian basis sets for accurate calculations on molecular systems in gas and condensed phases. *J. Chem. Phys.* **2007**, *127*, 114105.

(16) Grimme, S.; Antony, J.; Ehrlich, S.; Krieg, H. A consistent and accurate ab initio parametrization of density functional dispersion correction (DFT-D) for the 94 elements H-Pu. *J. Chem. Phys.* **2010**, *132*, 154104.

(17) Beck, A. D. Density-functional thermochemistry. III. The role of exact exchange. *J. Chem. Phys.***1993**, *98*, 5648-5656.

(18) Lee, C.; Yang, W.; Parr, R. G. Development of the Colle-Salvetti correlation-energy formula into a functional of the electron density. *Phys. Rev. B* **1988**, *37*, 785-789.

(19) Hargittai, M. Molecular structure of metal halides. *Chem. Rev.* **2000**, *100*, 2233-2301.

(20) Dudarev, S. L.; Botton, G. A.; Savrasov, S. Y.; Szotek, Z.; Temmerman, W. M.; Sutton, A. P. Electronic structure and elastic properties of strongly correlated metal oxides from first principles: LSDA + U, SIC-LSDA and EELS Study of UO_2 and NiO. *Phys. Status Solidi A* **1998**, *166*, 429-443.

(21) Nosé, S. A molecular dynamics method for simulations in the canonical ensemble. *Mol. Phys.* **1984**, *52*, 255-268.

(22) Head, J. D.; Zerner, M. C. A Broyden-Fletcher-Goldfarb-Shanno optimization procedure for molecular geometries. *Chem. Phys. Lett.* **1985**, *122*, 264-270.

(23) Limas, N. G.; Manz, T. A. Introducing DDEC6 atomic population analysis: Part 2. Computed results for a wide range of periodic and nonperiodic materials. *RSC Adv.* **2016**, *6*, 45727-45747.

(24) Limas, N. G.; Manz, T. A. Introducing DDEC6 atomic population analysis: Part 4. Efficient parallel computation of net atomic charges, atomic spin moments, bond orders, and more. *RSC Adv.* **2018**, *8*, 2678-2707.

(25) Manz, T. A.; Limas, N. G. Introducing DDEC6 atomic population analysis: Part 1. Charge partitioning theory and methodology. *RSC Adv.* **2016**, *6*, 47771-47801.

(26) Jónsson, H.; Mills, G.; Jacobsen, K. W. Nudged elastic band method for finding minimum energy paths of transitions. In *Classical and Quantum Dynamics in Condensed Phase Simulations*, World Scientific, 1998, Vol. 122, pp 385-404.

(27) Henkelman, G.; Jónsson, H. Improved tangent estimate in the nudged elastic band method for finding minimum energy paths and saddle points. *J. Chem. Phys.* **2000**, *113*, 9978-9985.

(28) Derrien, J. Y.; Dupuy, J. A structural analysis of the ionic liquids KCl and CsCl by neutron diffraction. *J. Phys. France* **1975**, *36*, 191-198.

(29) Badyal, Y. S.; Allen, D. A.; Howe, R. A. The structure of liquid $AlCl_3$ and structural modification in $AlCl_3$-MCl (M=Li, Na) molten salt mixtures. *J. Phys. Condens. Matter* **1994**, *6*, 10193-10220.

(30) Shilov, A. E.; Shul'pin, G. B. Activation of C-H Bonds by Metal Complexes. *Chem. Rev.* **1997**, *97*, 2879-2932.